

Evidence for Fermi surface reconstruction in the static stripe phase of $\text{La}_{1.8-x}\text{Eu}_{0.2}\text{Sr}_x\text{CuO}_4$, $x = 1/8$

V. B. ZABOLOTNYY^{1(a)}, A. A. KORDYUK^{1,2}, D. S. INOSOV^{1,3}, D. V. EVTUSHINSKY¹, R. SCHUSTER¹, B. BÜCHNER¹, N. WIZENT¹, G. BEHR¹, S. PYON⁴, T. TAKAYAMA⁴, H. TAKAGI⁴, R. FOLLATH⁵ and S. V. BORISENKO¹

¹ *Institute for Solid State Research, IFW-Dresden - P.O. Box 270116, D-01171 Dresden, Germany, EU*

² *Institute of Metal Physics of National Academy of Sciences of Ukraine - 03142 Kyiv, Ukraine*

³ *Max-Planck-Institute for Solid State Research - Heisenbergstraße 1, D-70569 Stuttgart, Germany, EU*

⁴ *Department of advanced materials, University of Tokyo - Kashiwanoha 5-1-5, Kashiwa 277-8561, Japan*

⁵ *Elektronenspeicherring BESSY II, Helmholtz-Zentrum Berlin für Materialien und Energie*

Albert-Einstein-Strasse 15, D-12489, Berlin, Germany, EU

received 17 February 2009; accepted in final form 30 April 2009

published online 3 June 2009

PACS 74.72.Dn – La-based cuprates

PACS 74.25.Jb – Electronic structure

PACS 74.81.-g – Inhomogeneous superconductors and superconducting systems

Abstract – We present a photoemission study of $\text{La}_{1.8-x}\text{Eu}_{0.2}\text{Sr}_x\text{CuO}_4$ with doping level $x = 1/8$, where the charge carriers are expected to order forming static stripes. Though the local probes in direct space seem to be consistent with this idea, there has been little evidence found for such ordering in quasiparticle dispersions. We show that the Fermi surface topology of the $1/8$ compound develops notable deviations from that observed for $\text{La}_{2-x}\text{Sr}_x\text{CuO}_4$ in a way consistent with the FS reconstruction expected for the scattering on the antiphase stripe order.

Copyright © EPLA, 2009

Since the discovery of charge- and spin-ordering in high- T_c cuprates, the phenomenon has attracted much attention, from the theoretical and experimental point of view [1–3]. Moreover, there appeared a number of theoretical approaches considering the charge and spin segregation as having strong, if not decisive, impact on the onset of superconductivity in high- T_c superconductors [4,5]. The ordering effects were found to depend crucially on the charge doping level, being the most pronounced for the pseudogap regime in the vicinity of doping level $x = 1/8$, where the doped holes are expected to form so-called stripes with the antiferromagnetically ordered spins.

Generally, the stripe order is supposed to fluctuate, though for particular superconductors such as $\text{La}_{2-x-y}\text{M}_x\text{Sr}_y\text{CuO}_4$ ($M = \text{Nd}$ or La) the inhomogeneities were shown to be practically static [6–13], making those compounds most prevalent in experimental research. The spin response of the stripe phase has been studied in inelastic neutron scattering experiments [6,14] supporting the idea of spin ordering. Similarly, local probes, such as scanning tunnelling microscopy, have clearly demonstrated charge modulation on the surface of high- T_c

superconductors [15,16], changing the hypothesis of spin and charge modulation into a well established fact.

On general grounds any charge/spin ordering must act as an additional scattering potential, resulting in a reconstruction of the initial Fermi surface (FS). Indirect evidence for such modifications comes from Hall coefficient and de Haas-van Alphen measurements [17–20], suggesting a formation of new orbits when the stripe order sets in. Nonetheless the experiments that would explicitly expose the effect of charge stripe order on the free charge carriers, namely modifications to the electronic band dispersion and topology of the FS, are not numerous and suggest different distribution of quasiparticle spectral weight over the Brillouin zone [21–24].

Here we present experimental data on the electronic band structure of $\text{La}_{1.675}\text{Eu}_{0.2}\text{Sr}_{0.125}\text{CuO}_4$ obtained using angle resolved photoelectron spectroscopy (ARPES) and compare the topology of the experimentally observed FS to that of pure $\text{La}_{2-x}\text{Sr}_x\text{CuO}_4$ (LSCO) samples and to a simple model, where electrons scatter on effective potential induced by the stripe and charge order. We show that the measured intensity distribution is consistent with the FS reconstruction expected for the antiphase stripe order [25–27] and give quantitative estimates for

^(a)E-mail: v.zabolotnyy@ifw-dresden.de

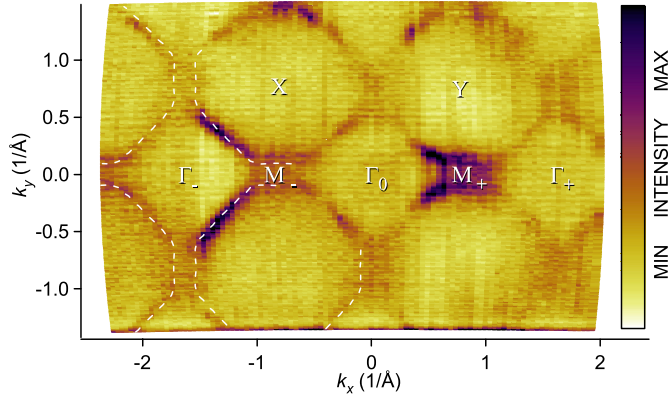


Fig. 1: (Colour on-line) Experimental FS map of $\text{La}_{1.675}\text{Eu}_{0.2}\text{Sr}_{0.125}\text{CuO}_4$, $T = 25$ K, $h\nu = 110$ eV. No symmetrization was applied, the map contains a set of independent \mathbf{k} points covering several Mahan cones [36].

the strength of the scattering potential in the spin and charge channels.

The experimental data in this report were collected at BESSY 1³ station using energy and momentum resolution of 12 meV and 0.05 \AA^{-1} respectively. The high-quality single crystals of $\text{La}_{1.675}\text{Eu}_{0.2}\text{Sr}_{0.125}\text{CuO}_4$ with suppressed superconductivity were mounted on the cryomanipulator and cleaved *in situ* in ultrahigh vacuum. All the Eu-LSCO data were collected at low temperature $T = 25$ K and measured with light polarization perpendicular to the analyzer entrance slit and excitation energy $h\nu = 110$ eV. Graphical representation of experimental geometry can be found elsewhere [28].

We start the discussion of the experimental data with the FS map plotted in fig. 1, which represents the photoelectron intensity integrated over a small energy window $E = E_F \pm 15$ meV. While for pure LSCO with the doping level $0.05 \lesssim x \lesssim 0.17$ the FS consists of the rounded contours centered at the X/Y points, for the Eu-doped sample the form of the FS contours is qualitatively different. There are extended and practically straight FS segments passing through the nodal points comprising 45° angle with the primary axes. At the antinodal point the apparent FS contour changes direction, forming segments parallel to the primary crystallographic axes, so that the whole FS rather reminds an octagon as shown by dotted guide lines in fig. 1. Assuming the observed contours represent a true connected FS we tried to fit it with a standard tight-binding (TB) formula [29]. It was practically impossible to find a set of TB parameters that would provide a reasonable fit both at the Fermi level (FL) as well as at higher binding energies. This was the first indication that the assumed topology of the FS is not a true one, *i.e.* the apparent FS may consist of several disjoint pockets, which in view of disorder introduced by Eu doping or/and short correlation length of the stripe potential are hard to detect. In some sense the situation may be similar to the electron doped cuprates, whose FS

undergoes reconstruction, though in the photoemission data the reconstructed FS consisting of the hole and electron pockets still resembles the unreconstructed one [30].

Nonetheless, we still tried to adhere to the idea of continuous contours and estimate the doping level from the FS area. As was mentioned, in this case the unusual TB formula does not provide a satisfactory fit with a reasonable number of fitting parameters. Therefore restricting a number parameters, as a model we used an octagon parameterized by two variables defining the distance from its center to the even and odd edges, respectively. The fit resulted in doping level of $x = 0.19 \pm 0.02$, which is notably higher than expected 0.125, and thus would be at variance with a reasonable agreement between the nominal doping level of the LSCO system and the one estimated by the FS area [29], unless we abandon the idea of continuous FS contours.

Other evidence for the discontinuity of the assumed FS contour comes from the analysis of the photoemission intensity over the whole measured range of binding energies. In fig. 2 we plot a series of energy-momentum cuts, representing photoelectron intensity for several fixed k_x values spanning from Γ_0 to M_1 point as a function of k_y and binding energy. In the first column one can clearly see two bands crossing the FL at $k_y \simeq \pm 0.3 \text{ \AA}^{-1}$. Were the assumed octagonal FS contours really continuous, one should see these two bands and corresponding FL crossings gradually moving closer to each other as k_x approaches the M point. Indeed the aforementioned FL crossings are getting slightly closer as it follows from the second column of fig. 2, but at $k_y = 0$ there appears another band that gains the intensity and finally results in a well defined FL crossing for the $k_x \gtrsim 0.6\Gamma_0M_+$, *i.e.* the FS segments at $k_x \lesssim 0.6\Gamma_0M_+$ and $k_x \gtrsim 0.6\Gamma_0M_+$ must belong to a separate FS sheet and the seeming continuity must be only due to the large momentum width of the features and specifics of the photoemission that make the FS segments that practically coincide with the “parent” FS the most intense and dominating over the replicas in the ARPES signal. Here one might get alarmed, lest the observed behavior should be an outcome of so called “waterfalls” [31] producing long tails below the dispersing bands as shown in second row of fig. 2. However, recalling that these high-energy features appear at $E \gtrsim 0.5$ eV, it would be hard to explain the presence of three peaks for the cut at $k_x = 0.38\Gamma_0M_+$ in the energy range $E = 100\text{--}200$ meV, as in that case there should have been three “waterfalls”, extending in unusual direction towards the FL. Similarly a suppression of photoemission intensity around high-symmetry direction $k_y = 0$ cannot be an alternative explanation, since it produces only one notch in the image instead of two. Therefore we regard the “waterfalls” as an unlikely explanation for the apparent discontinuity of the FS contour.

Along with the FS breaking into several sheets one would also expect characteristic back-folding effects in the

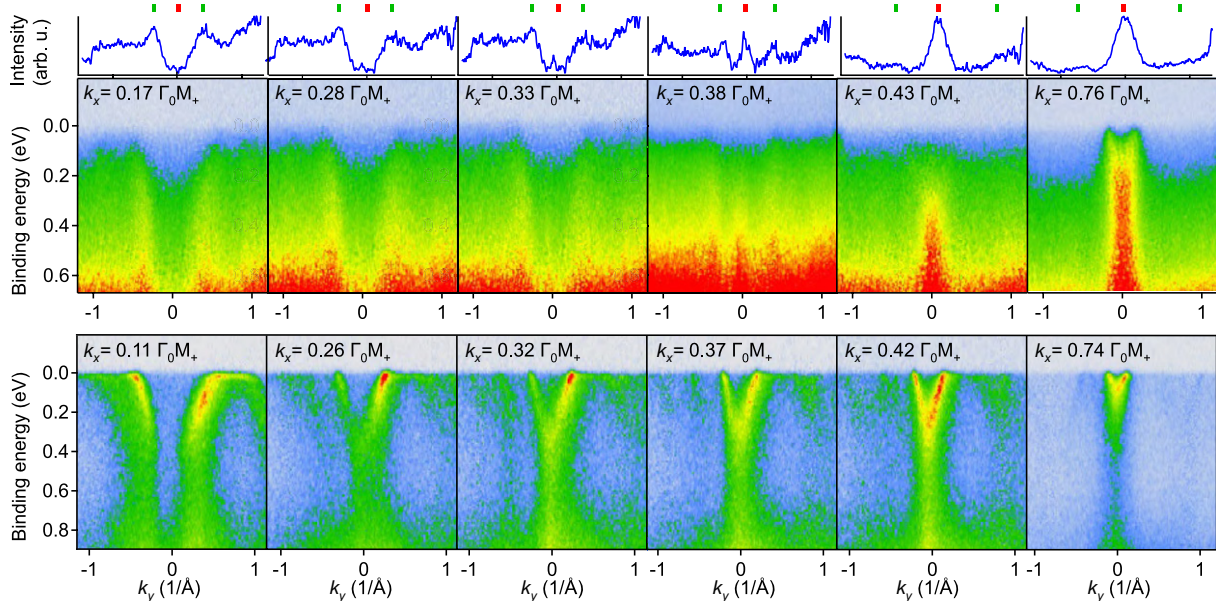


Fig. 2: (Colour on-line) Spectral weight evolution over the Brillouin zone. First row represents data set for $\text{La}_{1.675}\text{Eu}_{0.2}\text{Sr}_{0.125}\text{CuO}_4$ sample, the curves on top of each energy-momentum image are MDC integrated in the energy window 0.3–0.4 eV. To demonstrate possible influence of waterfalls [31], the second row contains similar data for Bi-2212 sample ($T_c = 70$ K) measured in the same experimental geometry. Unlike Eu-LSCO here the FL crossings continuously approach one another when moving closer to M point.

band dispersions. Nevertheless this kind of reasoning must be exploited cautiously as the coherence length of the folding potential and finite experimental resolution may result in notable deviation from the simple picture. It is well known that the FS of some electron doped cuprates is reconstructed, splitting into the hole and electron pockets [30]. The reason for this reconstruction is likely to be the short range antiferromagnetic correlations that appear for the electron doping $x \lesssim 0.14$. In fig. 3(a) we show a typical back-folded band for $\text{Pr}_{1.85}\text{Ce}_{0.15}\text{CuO}_4$. As it can be seen, the major signature of reconstruction can be described as the band having been “chopped off” above the line A-A (fig. 3(a)). Analogous effects can also be found in the energy-momentum intensity distribution for the Eu-LSCO sample (see fig. 3(b)), providing another indication for the FS reconstruction. There is nothing phenomenological in the appearance of the spectral function like been “chopped-off”. It results from effects of finite self energy, decaying intensity of the back-folded replica combined with experimental resolution, and can be easily reproduced by a model calculation as shown in fig. 3(d)–(f). Presence of the replica band can be also testified by usual MDC’s, as demonstrated for the experimental and model spectra in fig. 3(c) and (f), respectively.

One of the first easy-to-grasp consideration of the FS reconstructions due to the spin and charge modulation has been given in ref. [26], but focusing mainly on the Hall effect the authors restricted the discussion to the formal FS topology. When aiming at comparison to the photoemission experiment such a description needs to be extended, since these are not the bands that are seen

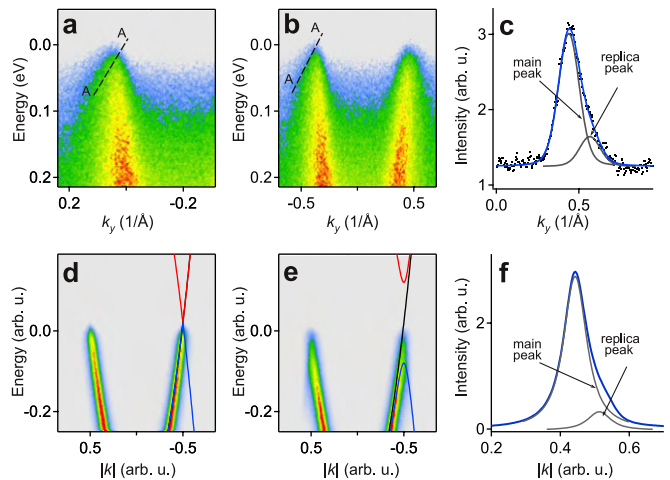


Fig. 3: (Colour on-line) Effect of band folding in experimental spectra of $\text{Pr}_{1.85}\text{Ce}_{0.15}\text{CuO}_4$ (a) and Eu-LSCO (b). (c) Asymmetric experimental MDC (black dots) for Eu-LSCO integrated in the energy window 22 ± 5 meV and its fit with two components corresponding to the main and replica bands. (d)–(e) Demonstration of band folding in the model spectra. (d) Zero scattering potential \Rightarrow zero gap, zero replica intensity. (e) Finite scattering \Rightarrow appearance of finite intensity of the back-folded replica and “chopped-off” form of the spectral function at the FL. (f) Decomposition of model MDC similar to (c).

directly in the photoemission experiment but the spectral function modified by the photoemission matrix elements $\Delta_{f,i}$. Even when the matrix elements can be neglected in the unreconstructed case, the intensity variations upon

the reconstruction are generally tremendous [32]. Typically one notes a significantly lower intensity of the newly sprang-up replicas as compared to the original unreconstructed bands. To understand this important and ubiquitous intensity disparity [32,33] one may turn to a sudden approximation as the simplest, but still sufficient for this purpose, approach. In this case the intensity of photoelectrons detected at some final state $|f\rangle$ can be written as [34]:

$$J_f(\omega) = f(\omega) \sum_i |\Delta_{f,i}|^2 A_i(\omega) = \sum_i |\Delta_{f,i}|^2 A_i^<(\omega). \quad (1)$$

Here the summation runs over the set of one-electron states $|i\rangle$ forming the basis in which the spectral function $A_i(\omega)$ is given. For our particular purpose, when considering a 2D cuprate, we reduce the complete basis set to states forming the single band crossing the FL, and naturally enumerate them by the Bloch quasi-momentum $\mathbf{k} = (k_x, k_y)$ limited to the unreconstructed BZ: $k_x \in [-\frac{\pi}{a}; +\frac{\pi}{a}]$, $k_y \in [-\frac{\pi}{b}; +\frac{\pi}{b}]$. Furthermore, we consider the excitations as a well defined quasiparticles and write the Hamiltonian in a diagonal form

$$\hat{H}_0 = \sum_{\mathbf{k} \in \text{BZ}} \varepsilon_{\mathbf{k}} \hat{c}_{\mathbf{k}}^\dagger \hat{c}_{\mathbf{k}}, \quad (2)$$

with $\varepsilon_{\mathbf{k}}$ being the renormalized band dispersion. It is easy to check that the spectral function reduces to a trail of delta functions aligned along the band dispersion [35], and that the matrix element $\Delta_{f,i}$ between the final state $|f\rangle$ characterized by the electron momentum \mathbf{p} and initial state $|i\rangle$ given by the Bloch wave with quasi-momentum \mathbf{k} ensures periodic replication of the photoemission picture determined by $A_{\mathbf{k}}(\omega)$ over different Mahan cones [36] as it can actually be seen in fig. 1.

As was pointed out in ref. [26], commensurate stripe order assumed in the model of antiphase stripe domains [25] induces additional potential due to scattering on spin and charge modulations $V = V_s + V_c$ that can be characterized by two most significant matrix elements

$$V_s = \langle \mathbf{k} | \hat{V}_s(\mathbf{r}) | \mathbf{k} \pm \mathbf{Q}_s \rangle, \quad \text{with } \mathbf{Q}_s = (3\pi/4; \pi), \quad \text{and} \quad (3)$$

$$V_c = \langle \mathbf{k} | \hat{V}_c(\mathbf{r}) | \mathbf{k} \pm \mathbf{Q}_c \rangle, \quad \text{with } \mathbf{Q}_c = (\pi/2; 0).$$

The choice of this particular model is motivated by the recent inelastic X-ray and neutron scattering experiments that seem to be in agreement with the theoretically expected vectors of charge modulations, not taking into account a small ($\sim 3\%$) incommensurability [37].

Introducing a quasi-momentum \mathbf{q} limited to the reduced Brillouin zone (RBZ) because of the enlarged unit cell in the real space, and zone number $m = 0, \dots, 7$, which becomes necessary to describe the states of the original band if the RBZ is used, the system Hamiltonian for the modulated case can be written as a matrix with respect to the zone index m :

$$\hat{H} = \sum_{\substack{\mathbf{q} \in \text{RBZ} \\ m, n = 0, \dots, 7}} (\delta_{m,n} \varepsilon_{\mathbf{q} + \mathbf{g}_m} + V_{m,n}) \hat{c}_{\mathbf{q} + \mathbf{g}_m}^\dagger \hat{c}_{\mathbf{q} + \mathbf{g}_n},$$

with

$$V_{m,n}(\mathbf{q}) = \begin{pmatrix} 0 & V_c & 0 & V_c & 0 & V_s & V_s & 0 \\ V_c & 0 & V_c & 0 & 0 & 0 & V_s & V_s \\ 0 & V_c & 0 & V_c & V_s & 0 & 0 & V_s \\ V_c & 0 & V_c & 0 & V_s & V_s & 0 & 0 \\ 0 & 0 & V_s & V_s & 0 & V_c & 0 & V_c \\ V_s & 0 & 0 & V_s & V_c & 0 & V_c & 0 \\ V_s & V_s & 0 & 0 & 0 & V_c & 0 & V_c \\ 0 & V_s & V_s & 0 & V_c & 0 & V_c & 0 \end{pmatrix}, \quad (4)$$

where \mathbf{g}_m is a set of 8 vectors determined by the condition $\mathbf{g}_m = k_m \mathbf{Q}_c + l_m \mathbf{Q}_s \in \text{BZ}$ and $k_m, l_m \in \mathbb{Z}$. Diagonalizing the matrix $H_{m,n}(\mathbf{q}) = \delta_{m,n} \varepsilon_{\mathbf{q} + \mathbf{g}_m} + V_{m,n}$ results in 8 eigenvalues and eigenstates for each particular $\mathbf{q} \in \text{RBZ}$:

$$\hat{H} = \sum_{\substack{\mathbf{q} \in \text{RBZ} \\ i, m, n = 0, \dots, 7}} D_{m,i}^*(\mathbf{q}) E_i(\mathbf{q}) D_{i,n}(\mathbf{q}) \hat{c}_{\mathbf{q} + \mathbf{g}_m}^\dagger \hat{c}_{\mathbf{q} + \mathbf{g}_n} = \sum_{\substack{\mathbf{q} \in \text{RBZ} \\ i = 0, \dots, 7}} E_i(\mathbf{q}) \hat{a}_{\mathbf{q},i}^\dagger \hat{a}_{\mathbf{q},i}, \quad (5)$$

where

$$\hat{a}_{\mathbf{q},i} = \sum_n D_{i,n}(\mathbf{q}) \hat{c}_{\mathbf{q} + \mathbf{g}_n}.$$

Now, knowing the eigenstates $\hat{a}_{\mathbf{q},i}^\dagger |0\rangle$ and eigenenergies $E_i(\mathbf{q})$ of the reconstructed system we write the spectral function

$$\begin{aligned} A_{\mathbf{k}}^<(\omega) &= \sum_{\substack{\mathbf{q} \in \text{RBZ}, \\ i = 0, \dots, 7}} \left| \langle 0 | \hat{c}_{\mathbf{k}} | \mathbf{q}, i \rangle \right|^2 \delta(E_i(\mathbf{q}) - \omega) = \\ &= \sum_{\substack{\mathbf{q} \in \text{RBZ}, \\ i, m = 0, \dots, 7}} \left| \langle 0 | \hat{c}_{\mathbf{k}} D_{m,i}^*(\mathbf{q}) \hat{c}_{\mathbf{q} + \mathbf{g}_m}^\dagger | 0 \rangle \right|^2 \delta(E_i(\mathbf{q}) - \omega) = \\ &= \sum_{\substack{\mathbf{q} \in \text{RBZ}, \\ i, m = 0, \dots, 7}} \left| D_{m,i}^*(\mathbf{k} - \mathbf{g}_m) \right|^2 \delta(E_i(\mathbf{k} - \mathbf{g}_m) - \omega). \end{aligned} \quad (6)$$

From the last formula it can be easily seen that for the case of infinitesimally small potential $V_{n,m}(\mathbf{q})$ the reconstructed band structure must consist of 8 ‘‘replicas’’ obtained from the original structure shifted by vectors \mathbf{g}_m with the distribution of the spectral weight determined by the components of eigenvectors $D_{m,i}(\mathbf{k} - \mathbf{g}_m)$, which results in an infinitesimally small intensity of all the replicas that do not overlap with the original structure. In case of scattering potential values comparable to the band width of the original structure the general property of weak replica intensities remains valid, though the evaluation of the spectral function must be done numerically. To check whether the experimental FS can be reproduced within the discussed model, we have calculated the spectral weight distributions for different spin and charge scattering potentials. The obtained distributions are shown in fig. 4. Before comparing the calculated FS to the experimental one we have to mention that in the model we have preserved the anisotropy of the stripe scattering potential, while in the experimental data one is likely to observe

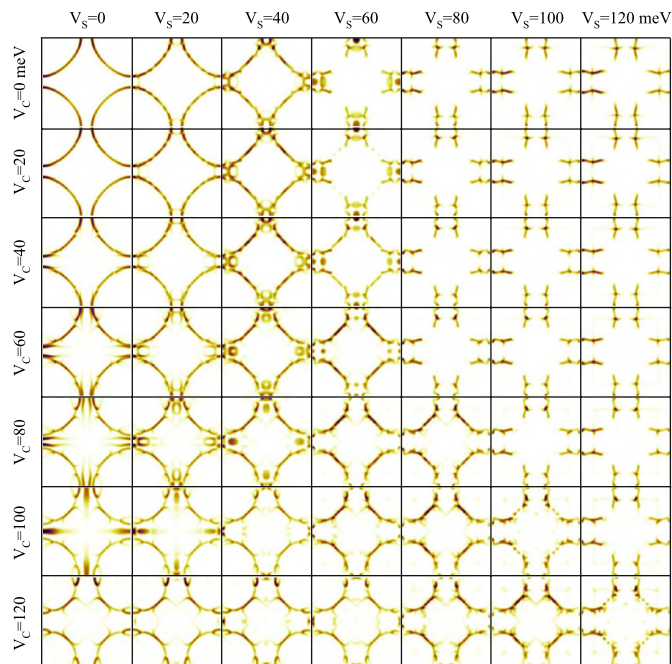


Fig. 4: (Colour on-line) Calculated FS for various scattering potentials V_c and V_s . Calculated spectral function was smoothed within small energy and momentum windows to simulate experimental resolution and averaged over two possible stripe orientations.

coexistence of stripes running along the x - and y -direction. Thus when searching for the optimal values of $V_{s,c}$ we should not sift out the calculated spectra just because of their apparent one-dimensionality. From the fig. 4 it is obvious that there is no problem for the model to reproduce the seeming octagonal structure of the experimental FS, though the values of spin scattering exceeding 80 meV are surely too large. Further restriction on the values of $V_{s,c}$ can be drawn comparing distances between the most intense part in the intensity distributions. Our subjective judgement for the nearest fit to the experimental data would be the case of $V_s \approx 60 \pm 20$ and $V_c \approx 100 \pm 20$ meV.

When further comparing the model to the experimental data the issue of the stripe scattering potential periodicity has to be mentioned. This seems to be especially important for the problem of a pseudogap that has been observed in a similar type of stripe compound [22]. Strictly speaking both charge and spin order are not commensurate to the lattice and have finite correlation lengths [37], which certainly must affect the finer details in the electronic structure. From studies of quasicrystals and quasi-periodic alloys it has been known for decades that incommensurate potentials generally lead to suppression of the spectral weight at the FL, which in that field of research has also been termed as “pseudogap” [38–40]. Hence we would like to draw reader’s attention to the suppressed spectral weight in the energy range up to 300 meV, which become especially spectacular when

compared to Bi-2212 case. Recalling the whole bulk of currently available spectroscopic data it even might be tempting to generalize this for the whole La-214 family. In any case, a detailed comparative study appears to be very encouraging.

Here one may argue that there is no need to invoke any effects of incommensurability, and that the observed effects can be nicely explained by incoherence or fluctuation of preformed Cooper pairs [22]. However recalling that the maximal superconducting gap for LSCO hardly exceeds 20–30 meV, while the suppression of spectral weight in Eu-LSCO extends up to 200–300 meV, it is hardly believable that one can design an intelligible explanation without befogging the whole issue.

At the same time there are known successful attempts to transfer the ideas developed for the quasicrystals onto the problem of mysterious pseudogap in cuprates [41]. Recently a pseudogap effect, similar to the one discussed in high- T_c cuprates, has been detected in the incommensurate CDW phase of TaSe₂ [32] once again suggesting that the incommensurate order might be a long sought common origin of the pseudogaps. Unfortunately a precise calculation of rational approximates to the incommensurate structure is encumbered with drastically increased numeric complexity, although it is obvious that such a calculation would significantly help to understand the pseudogap formation mechanism in high-temperature superconducting cuprates.

This project is part of the Forschergruppe FOR538 and is supported by the DFG under Grants No. KN393/4 and BO1912/2-1. We thank R. HÜBEL for technical support.

REFERENCES

- [1] KIVELSON S. A., BINDLOSS I. P., FRADKIN E., OGANESYAN V., TRANQUADA J. M., KAPITULNIK A. and HOWALD C., *Rev. Mod. Phys.*, **75** (2003) 1201.
- [2] CASTRO NETO A. H. and SMITH C. M., arXiv:cond-mat/0304094 (2003).
- [3] CASTRO NETO A. H. and SMITH C. M., *Strong Interactions in Low Dimensions* (Kluwer) 2004.
- [4] VOJTA M., *Phys. Rev. B*, **66** (2002) 104505.
- [5] MARTIN I., ORTIZ G., BALATSKY A. V. and BISHOP A. R., *Europhys. Lett.*, **56** (2001) 849.
- [6] TRANQUADA J. M., STERNLIEB B. J., AXE J. D., NAKAMURA Y. and UCHIDA S., *Nature (London)*, **351** (1995) 561.
- [7] KLAUSS H.-H., WAGENER W., HILLBERG M., KOPMANN W., WALF H., LITTERST F. J., HÜCKER M. and BÜCHNER B., *Phys. Rev. Lett.*, **85** (2000) 4590.
- [8] KOJIMA K. M., EISAKI H., UCHIDA S., FUDAMOTO Y., GAT I. M., KINKHABWALA A., LARKIN M. I., LUKE G. M. and UEMURA Y. J., *Physica B: Condens. Matter*, **289-290** (2000) 343.

- [9] HUNT A. W., SINGER P. M., THURBER K. R. and IMAI T., *Phys. Rev. Lett.*, **82** (1999) 4300.
- [10] TEITEL'BAUM G. B., BÜCHNER B. and DE GRONCKEL H., *Phys. Rev. Lett.*, **84** (2000) 2949.
- [11] KATAEV V., RAMEEV B., VALIDOV A., BÜCHNER B., HÜCKER M. and BOROWSKI R., *Phys. Rev. B*, **58** (1998) R11876.
- [12] SUH B. J., HAMMEL P. C., HÜCKER M., BÜCHNER B., AMMERLAHL U. and REVCOLEVSCHI A., *Phys. Rev. B*, **61** (2000) R9265.
- [13] SIMOVIĆ B., HAMMEL P. C., HÜCKER M., BÜCHNER B. and REVCOLEVSCHI A., *Phys. Rev. B*, **68** (2003) 012415.
- [14] TRANQUADA J. M., AXE J. D., ICHIKAWA N., MOODENBAUGH A. R., NAKAMURA Y. and UCHIDA S., *Phys. Rev. Lett.*, **78** (1997) 338.
- [15] HOFFMAN J., HUDSON E. W., M. L. K., MADHAVAN V., EISAKI H., UCHIDA S. and DAVIS J. C., *Science*, **295** (2002) 5554.
- [16] VERSHININ M., MISRA S., ONO S., ABE Y., ANDO Y. and YAZDANI A., *Science*, **303** (2004) 1995.
- [17] LEBOEUF D., DOIRON-LEYRAUD N., LEVALLOIS J., DAOU R., BONNEMAISON J.-B., HUSSEY N. E., BALICAS L., RAMSHAW B. J., LIANG R., BONN D. A., HARDY W. N., ADACHI S., PROUST C. and TAILLEFER L., *Nature (London)*, **450** (1995) 533.
- [18] ADACHI T., NOJI T. and KOIKE Y., *Phys. Rev. B*, **64** (2001) 144524.
- [19] NAKAMURA Y. and UCHIDA S., *Phys. Rev. B*, **46** (1992) 5841.
- [20] SEBASTIAN S. E., HARRISON N., PALM E., MURPHY T. P., MIELKE C. H., LIANG R., BONN D. A., HARDY W. N. and LONZARICH G. G., *Nature (London)*, **454** (2008) 200.
- [21] ZHOU X. J., BOGDANOV P., KELLAR S. A., NODA T., EISAKI H., UCHIDA S., HUSSAIN Z. and SHEN Z.-X., *Science*, **286** (1999) 268.
- [22] VALLA T., FEDOROV A. V., LEE J., DAVIS J. C. and GU G. D., *Science*, **314** (2006) 1914.
- [23] FENG D. L., LU D. H., SHEN K. M., OH S., ANDRUS A., O'DONNELL J., ECKSTEIN J. N., ICHI SHIMOYAMA J., KISHIO K. and SHEN Z. X., *Physica C: Superconductivity*, **341-348** (2000) 2097.
- [24] HE R.-H., TANAKA K., MO S.-K., SASAGAWA T., FUJITA M., ADACHI T., MANNELLA N., YAMADA K., KOIKE Y., HUSSAIN Z. and SHEN Z.-X., *Nat. Phys.*, **5** (2009) 119.
- [25] ZAAANEN J. and GUNNARSSON O., *Phys. Rev. B*, **40** (1989) 7391.
- [26] MILLIS A. J. and NORMAN M. R., *Phys. Rev. B*, **76** (2007) 220503.
- [27] MACHIDA K., *Physica C: Superconductivity*, **158** (1989) 192.
- [28] INOSOV D. S., SCHUSTER R., KORDYUK A. A., FINK J., BORISENKO S. V., ZABOLOTNYY V. B., EVTUSHINSKY D. V., KNUPFER M., BÜCHNER B., FOLLATH R. and BERGER H., *Phys. Rev. B*, **77** (2008) 212504.
- [29] YOSHIDA T., ZHOU X. J., TANAKA K., YANG W. L., HUSSAIN Z., SHEN Z.-X., FUJIMORI A., SAHRKORPI S., LINDROOS M., MARKIEWICZ R. S., BANSIL A., KOMIYA S., ANDO Y., EISAKI H., KAKESHITA T. and UCHIDA S., *Phys. Rev. B*, **74** (2006) 224510.
- [30] PARK S. R., ROH Y. S., YOON Y. K., LEEM C. S., KIM J. H., KIM B. J., KOH H., EISAKI H., ARMITAGE N. P. and KIM C., *Phys. Rev. B*, **75** (2007) 060501.
- [31] INOSOV D. S., FINK J., KORDYUK A. A., BORISENKO S. V., ZABOLOTNYY V. B., SCHUSTER R., KNUPFER M., BÜCHNER B., FOLLATH R., DÜRR H. A., EBERHARDT W., HINKOV V., KEIMER B. and BERGER H., *Phys. Rev. Lett.*, **99** (2007) 237002.
- [32] BORISENKO S. V., KORDYUK A. A., YARESKO A. N., ZABOLOTNYY V. B., INOSOV D. S., SCHUSTER R., BÜCHNER B., WEBER R., FOLLATH R., PATTHEY L. and BERGER H., *Phys. Rev. Lett.*, **100** (2008) 196402.
- [33] BROUET V., YANG W. L., ZHOU X. J., HUSSAIN Z., RU N., SHIN K. Y., FISHER I. R. and SHEN Z. X., *Phys. Rev. Lett.*, **93** (2004) 126405.
- [34] HEDIN L. and LEE J. D., *J. Electron Spectrosc. Relat. Phenom.*, **124** (2002) 289.
- [35] MAHAN G. D., *Many Particle Physics* (Plenum Press) 1981.
- [36] MAHAN G. D., *Phys. Rev. B*, **2** (1970) 4334.
- [37] KIM Y.-J., GU G. D., GOG T. and CASA D., *Phys. Rev. B*, **77** (2008) 064520.
- [38] WU X., KYCIA S. W., OLSON C. G., BENNING P. J., GOLDMAN A. I. and LYNCH D. W., *Phys. Rev. Lett.*, **75** (1995) 4540.
- [39] HAFNER J. and KRAJČÍ M., *Phys. Rev. Lett.*, **68** (1992) 2321.
- [40] UEDA K. and TSUNETSUGU H., *Phys. Rev. Lett.*, **58** (1987) 1272.
- [41] SEIBOLD G., BECCA F., BUCCI F., CASTELLANI C., CASTRO C. D. and GRILLI M., *Eur. Phys. J. B*, **13** (2000) 87.